MEASUREMENTS AND CALCULATIONS OF FIELD DISTRIBUTIONS IN SHORT HELICAL RESONATORS*

by

T. A. Tombrello and K. S. Jancaitis
California Institute of Technology
Pasadena, California 91109
and
P. J. Bendt, B. H. Erkkila, and R. H. Stokes
Los Alamos Scientific Laboratory,
University of California
Los Alamos, New Mexico 87544

ABSTRACT

The simple conducting sheath model of the helical waveguide accurately describes the properties of both helical transmission lines and long helix resonators. However, the boundary conditions at the ends of a resonator are not satisfied exactly for the coupled TE-TM mode solutions that arise in the sheath model treatment. The termination effects become more important for shorter resonators, and measurements of field distributions and resonant frequencies of half-wavelength resonators show large disagreements with simple sheath model calculations. Because of the interest in resonators of this type for low velocity linear accelerator structures, we have made an experimental and theoretical study of several short resonator geometries. A new calculational technique has been developed to describe the boundary conditions more accurately. Comparisons with measured electric and magnetic field distributions and resonant frequencies for two half wavelength resonators are given. These comparisons demonstrate that the new method of calculation is a significant improvement over the simple sheath model.

---

*Work performed under the auspices of the U. S. Atomic Energy Commission and supported in part by the National Science Foundation (GP-28027).

I. INTRODUCTION

The use of helical waveguides for accelerating heavy particles has been discussed extensively in the literature.[1,2,3] Recent interest in this field has been based primarily on the low phase velocities that are possible in these structures, which seem especially appropriate for heavy ion acceleration. Interest in alternating phase focusing, and in building linacs with a variable velocity profile has shown that there are good reasons for constructing the accelerator from separately phased, short structures.[3,4] For helices, the most flexibility is obtained through use of the shortest possible elements, i.e. $\lambda/2$ resonators. A heavy ion accelerator has been proposed by the Los Alamos Scientific Laboratory based on the use of $\lambda/2$ helical resonators operating with independent phasing. Since these short resonators show maximum deviation from the predictions of available models there has been a need for experimental and theoretical studies. In early 1971, a program of helix resonator measurements was started at Los Alamos, with emphasis placed on short resonators which would accelerate heavy ions in the velocity range 2-8 percent of the velocity of light. Helix resonators with acceptable efficiencies for such slow particles operate at rather low frequencies. The combination of low frequency and small transverse dimensions also makes these resonators attractive possibilities for injectors or post-accelerators for cyclotrons.

The most straightforward mathematical description of the helical waveguide has been obtained using the sheath model, in which the helical coil is approximated by an anisotropic conducting layer of the same pitch as the actual coil.[5,6] Nearly all helix calculations have been based on this model, except for loss calculations where effects due to the finite size of the conductor in the helix are added in the form of local field enhancements.[3,7] It has been shown that the spatial variation of the accelerating field from the sheath model accurately reproduces the measured field shape when the length of the helical coil is large compared to the wavelength of the electromagnetic field in the cavity. The measurements, however, show large deviations near the ends of the coil.[7,8] These deviations must necessarily occur because the coupled TE-TM mode that satisfies the boundary conditions at the helix does not automatically satisfy the boundary conditions at the point where the helix is grounded.

In an attempt to overcome this difficulty, Sierk added decaying waveguide fields (beyond cutoff) to the basic sheath field.[9] Though this technique allows considerable improvement in the value obtained for the lowest resonant frequency, the representation of the electromagnetic field is poor, probably because of convergence difficulties. The individual decaying waveguide field components are not orthogonal to the sheath field, and thus a unique decomposition of this type is not possible. However, one would expect the non-sheath corrections to be small, and the success of the convergence will be determined mainly by how accurately the added field components provide these corrections.

It is the purpose of this paper to compare a new calculational technique with data from $\lambda/2$ helical resonators, and to demonstrate that a significantly better accuracy can be obtained than with previous calculational methods.

II. EXPERIMENT

A helical resonator is formed by placing a conducting coil inside a concentric conducting cylinder as shown in Fig. 1. For radiofrequency tests, resonators were constructed entirely of copper, and had end plates which were clamped in place during the measurements. To form the helix, a lathe was used to wind copper tubing onto a mandrel. The mandrel had grooves cut with the proper pitch and the conductor was guided onto the mandrel using the axial feed mechanism of the lathe. Both of the resonators discussed in the paper had helical conductors constructed with 0.64-cm diameter copper tubing. They were terminated as shown in Fig. 1 by hard soldering the tubing into the outer cylinder.

Measurements of the electric and magnetic fields in the resonators were made at low power levels by a perturbation method.[10] The total E^2 field as a function of position along the z-axis was obtained by pulling a 0.95-cm diameter sapphire bead through the resonator with a nylon thread. Before the bead enters the resonator the oscillator frequency is set exactly equal to the fundamental resonant frequency, so there is no phase difference

between the exciting antenna and the resonator electric fields. A vector voltmeter is used to observe the phase shift of the resonator fields relative to the oscillator as a function of bead position. The resonator phase was sampled with a lightly coupled probe inserted through the outer cylindrical wall. The following equation relates the phase shift ζ to E^2 at the location of the bead,

$$\tan \zeta = - \frac{3}{2} \omega_o V \varepsilon_o \left(\frac{\kappa-1}{\kappa+2}\right) \frac{E^2}{P}$$

where ω_o is the resonant angular frequency, and ε_o is the dielectric constant of free space. V is the volume of the perturbing bead, κ the specific inductive capacity of the bead, and P is the power dissipated in the resonator. An electric motor drive pulled the bead through the resonator at a constant speed, and a coupled helipot provided a voltage proportional to bead displacement. An X-Y recorder was used to plot the phase shift versus position of the bead. The shunt impedance can be obtained by integrating the square root of tan ζ along the resonator axis. Typical values lie in the range 15-25 megohms per meter.

The field components E_z^2, E_r^2, B_z^2, and B_r^2 were determined by pulling 0.84-cm diameter discs of 0.005-cm aluminum foil mounted on nylon threads, along various paths parallel to the axis of the resonator. The discs selectively perturb both the component of the B field perpendicular to the plane of the disc and the components of the E field which are in the plane of the disc. The B field can be distinguished from the E field because the resulting phase shifts have opposite signs. For a given path, phase shifts were measured for three orientations of the aluminum discs perpendicular to the three cylindrical coordinates. Each orientation yielded a curve of phase shift versus z that was a linear combination of the squares of the appropriate field components. Neglecting the effect of E_ϕ^2 and B_ϕ^2, which are expected to be very small, the components E_r^2, E_z^2, B_r^2, and B_z^2 could be obtained by taking differences between the three curves. To obtain accurate results it is essential that the ratio of the thickness to diameter of the perturbing disc be very small (< 0.01).[10]

III. THEORY

To describe the helix resonator, we define a cylindrical coordinate system so that the z axis lies along the common axis of the coil and the outer cylinder; the r and ϕ coordinates then lie in a plane perpendicular to this axis. (Refer to Fig. 1.) The helix has a constant radius "a," and the radius of the outer cylinder is "c." To support the helical coil, it is terminated as shown in Fig. 1. We mathematically idealize this by imposing ground planes at the ends of the helix (z=0 and z=L) which cut through the anisotropic conducting layer that represents the coil in the sheath approximation. This mathematical idealization is obviously different from the real termination.

Because we are chiefly interested in the lowest mode, we consider only those solutions that have no ϕ dependence. (The inclusion of the ϕ-dependent solutions requires only a trivial modification of the following treatment.)

The boundary conditions that $\vec{E}$ and $\vec{B}$ must satisfy in the sheath model[5] are given below.

At r=c: $E_z = B_r = E_\phi = 0$.

At r=a: $E_z + E_\phi \cot \Theta = 0$,
E_z and E_ϕ are continuous,
$B_z + B_\phi \cot \Theta$ is continuous.
($\cot \Theta = 2\pi a/s$)

At z=0 and Z=L: $E_r = E_\phi = B_z = 0$.

In order to satisfy the boundary conditions exactly at z=0 and L, we choose the following forms for E_z and B_z, with an assumed $e^{i\omega t}$ time dependence:

For r < a: $$E_z(r,z) = \sum_{n=1}^{\infty} \alpha_n I_o (g_n r) \cos \left(\frac{n\pi z}{L}\right)$$

and $$B_z(r,z) = \sum_{n=1}^{\infty} \beta_n' I_o (g_n r) \sin \left(\frac{n\pi z}{L}\right).$$

For r > a:

$$E_z(r,z) = \sum_{n=1}^{\infty} [\gamma_n I_o(g_n r) + \delta_n K_o (g_n r)] \cos \left(\frac{n\pi z}{L}\right),$$

$$B_z(r,z) = \sum_{n=1}^{\infty} [\rho_n I_o(g_n r) + \lambda_n K_o (g_n r)] \sin \left(\frac{n\pi z}{L}\right).$$

The quantity g_n is given by $\sqrt{(\frac{n\pi}{L})^2 - \kappa^2}$ and κ is the free space wave number ($\kappa = \omega/c$). The I_o and K_o are the Bessel functions of an imaginary argument. (The standard sheath model treatment[3,6] essentially corresponds to using just the first term in the E_z expression.)

The other components of E and B can easily be obtained from E_z and B_z using Maxwell's equations. The boundary conditions at r=c relate δ_n to γ_n and λ_n to ρ_n. Then, at r=a, α_n may be connected to γ_n and β_n' to ρ_n. Finally, the two other conditions at r=a give the following equations:

$$\sum_{n=1}^{\infty} \alpha_n I_o(g_n a) \cos\left(\frac{n\pi z}{L}\right) + (-i\kappa)\cot\theta \sum_{n=1}^{\infty} \frac{\beta_m'}{g_n^2} I_o'(g_n a) \sin\left(\frac{n\pi z}{L}\right) = 0,$$

and

$$\sum_{n=1}^{\infty} \left\{ \beta_n' A_n \sin\left(\frac{n\pi z}{L}\right) + i\kappa\cot\theta \frac{\alpha_n}{g_n^2} B_n \cos\left(\frac{n\pi z}{L}\right) \right\} = 0$$

where A_n and B_n are combinations of I_0, I_1, K_0 and K_1 evaluated at r = a and r = c.[11]

If we multiply the first equation above by $\cos\left(\frac{m\pi z}{L}\right)$ and the second by $\sin\left(\frac{m\pi z}{L}\right)$ and integrate from z=0 to z=L, we then obtain:

$$\alpha_m + \sum_{n=1}^{\infty} Q_{mn} \beta_n = 0,$$

and

$$\beta_m + \sum_{n=1}^{\infty} P_{mn} \alpha_n = 0.$$

In these equations we have replaced $i\beta_n'$ by β_n:

$$Q_{mn} = -\frac{2\kappa}{\pi} \frac{1}{g_n} \frac{I_1(g_n a)}{I_o(g_m a)} G(m,n),$$

$$P_{mn} = \frac{2\kappa}{\pi} \frac{g_m}{g_n^2} \frac{I_o(g_n c)}{I_1(g_m c)} X \left[\frac{I_1(g_m c)\, K_1(g_m a) - I_1(g_m a)\, K_1(g_m c)}{I_o(g_n a)\, K_o(g_n c) - I_o(g_n c)\, K_o(g_n a)} \right] G(m,n)$$

and

$$G(m,n) = \frac{\pi}{L} \int_o^L \cos\left(\frac{m\pi z}{L}\right) \cot\theta \sin\left(\frac{n\pi z}{L}\right) dz$$

We now see the advantage of taking separate expansions of E_z and B_z: not only are the boundary conditions at the ends of the helix exactly satisfied, but the boundary conditions at the helix yield a linear set of equations. To find a solution we truncate the summation to N non-zero terms; since the system is homogeneous, the condition that the determinant vanish gives a dispersion relation for the eigenfrequencies. Setting $\alpha_1 = 1$, we can solve for the remaining α's and β's.

It should be noticed that no assumption has been made concerning the z-dependence of cot θ, so that cases with variable pitch are included automatically. If cot θ is symmetric about the center of the cavity, the system splits into two separate homogeneous sets of equations; the even α's couple only to the odd β's and vice versa.

The calculation just described considers the expansion of the electromagnetic fields in the full cavity and henceforth will be referred to as the "full" approximation. As a method of checking the accuracy of this technique, another calculation has been made under more restricted conditions. This second case considers only the fields in half the cavity (z=0 to z=L/2), and thus can allow only variations in pitch that are symmetric about the center of the cavity.

This calculation will be referred to as the "half" approximation. For convenience the point z=0 will now be taken at the center of the cavity; thus, the grounded end is at z=L/2. To satisfy the boundary conditions at z=L/2, we must now expand E_z in a sine series and B_z in a cosine series. For example, at r < a:

$$E_z = \sum_{n=1}^{2N-1} \alpha_n I_o(g_n r) \sin\left(\frac{n\pi z}{L}\right)$$

and

$$B_z = \sum_{n=1}^{2N-1} \beta_n' I_o(g_n r) \cos\left(\frac{n\pi z}{L}\right)$$

where the boundary condition at z=L/2 requires that the summations be only over odd n. We now find that a given α_n couples directly to β_n. The α's in the "full" approximation are simply related to those of the "half" approximation:

$$\alpha_{3,\,\text{full}} = -\alpha_{3,\,\text{half}};$$

$$\alpha_{5,\ \text{full}} = \alpha_{5,\ \text{half}} ;$$

$$\alpha_{7,\ \text{full}} = -\alpha_{7,\ \text{half}} ;$$

The reader will note that in the development of the theory, no free parameters have been introduced. Thus, having specified the dimensions of the helix the resonant frequencies and the coefficients in the expansions of the fields are uniquely determined.

V. COMPARISON OF THE EXPERIMENTAL AND THEORETICAL RESULTS

In this section we shall compare the calculations described in the previous section with the field measurements discussed in Section II. The dimensions of the resonators and their resonant frequencies in the lowest mode are given in Table I together with the frequency prediction of the standard sheath model. These particular examples were chosen because they show how the electromagnetic properties change with the dimensions. The agreement with our calculations is neither better nor worse for these resonators than for other devices that have not been described in this paper. Thus, these results are typical of a wide range of helical resonator types.

In comparing the calculations to the data we have not taken into account the finite size of the perturbing bead or disk. For most of the results this introduces little error; however, near the end wall of the cavity where the bead or disk begins to enter the exit hole, the measurements are probably appreciably smaller than the actual fields.

In the figures we have chosen to present only the fields in half of each resonator. Since data were available over the whole range in z, the experimental curves shown are averages of the results in the two halves. This was done to eliminate the slight asymmetries (typically a few percent in the square of the field) that result from imperfections in the winding or positioning of the helix.

A. Resonator A

Only the axial field, $E_z(0,z)$, and the resonant frequency were measured for this resonator. The experimental value of the axial field is shown in Fig. 2, where it is compared with results given by the two approximations described in the previous section and with that from the standard sheath model. Table I shows how the α's and the calculated resonant frequency depend upon N. The similarity of the results for N=5 and N=10 indicate that the convergence of both approximations is adequate.

It is clear that both methods agree quite well and represent a decided improvement over the standard sheath model treatment. The deviation of the calculated curves from the data near the end of the helix (Fig. 2) is a manifestation of the difference between the mathematical and the actual boundary conditions at the termination.

B. Resonator B

The second example shows how the fields change when the radius of the helix becomes larger relative to its length. The experimental and calculated values of the fields are shown in Fig. 3 and 4; the α's and the calculated resonant frequency are given in Table I.

As described in Section II, the use of a thin, conducting disk for perturbation measurements allows the values of the squares of the individual field amplitudes to be deduced approximately. Since the calculations for this resonator indicate that the ϕ components of the fields should be quite small ($|E_{\phi,\max}(a)|/|E_{z,\max}(0)| \simeq .03$ and $|B_{\phi,\max}(a)|/|E_{z,\max}(0)| \simeq .07$), we have neglected E_ϕ^2 and B_ϕ^2 and used the measurements to determine E_r^2, E_z^2, B_r^2, B_z^2. These results are shown in Figs 3 and 4 (solid curves), where they are compared with the results of the "full" approximation. In each figure the calculations are normalized only to the maximum value of the field at r=0; the vertical scales thus give the correct relative magnitudes of the squares of the field components. The "half" approximation results are not given because "half" by its nature cannot give a reasonable description of B_r. Though $E_z(0,z)$ was slightly better for "half" than "full", the curves for E_z^2 and E_r^2 at the two other radii were in significantly better agreement for "full".

The fact that the calculated B_r has a larger peak near the end of the helix may result because

a few of the magnetic field lines in an actual side terminated resonator are free to emerge from the end of the helix. The measured fields shown beyond the end of the helix provide qualitative support of this interpretation. In addition, the magnitudes of the measured fields within 0.4 cm of the end wall of the cavity are strongly affected by the finite size of the disk, because in this region the disk starts to enter the exit hole in the wall. Thus, the actual fields are probably appreciably larger in this region and probably do not drop to zero in the way indicated by the measurements. The shape of the experimental curve for B_z^2 at r=6.67 cm also deviates from the calculated curve. However, since B_z^2 must be extracted from the data after two subtractions, it is not clear that the disagreement is significant.

Though the agreement is far from perfect, with the exception of the peak in B_r near the end of the helix, the theory gives an adequate description of the fields in the resonator. The reader will note that since the squares of the fields are plotted in Figs. 3 and 4, the disagreement between theory and experiment is magnified.

VI. REFERENCES

1. W. Muller and J. Rembser, Nucl. Instr. Meth., 4, 202 (1959).
2. H. Klein, P. Junior, J. Klabunde, O. Siart, H. Deitinghoff, P. Finke, and A. Schempp, Proceedings of the International Conference on Nuclear Reactions Induced by Heavy Ions (American Elsevier Publishing Co., New York, 1970) p. 491.
3. A. J. Sierk, C. J. Hamer, and T. A. Tombrello, Particle Accelerators, 2, 149 (1971).
4. I. Ben-Zvi, J. G. Castle and P. H. Ceperley, IEEE Trans. on Nuc. Sci., NS-19, No. 2, 226 (1972); H. F. Glavish, Ibid., 307 (1972).
5. J. R. Pierce, Traveling Wave Tubes (D. Van Nostrand Co., New York, 1950).
6. J. H. Bryant, Electrical Communication 31, 50 (1954).
7. H. Klein, N. Merz, and O. Siart, Particle Accelerators 3, 235 (1972).
8. C. M. Jones, J. P. Judish, R. F. King, S. K. McGowan, W. T. Milner and P. Z. Peebles, Particle Accelerators 3, 103 (1972).
9. A. J. Sierk, IEEE Trans. on Nuc. Sci., NS-18, No. 3, 162 (1971).
10. E. L. Ginzten, "Microwave Measurements" (McGraw-Hill Book Co., Inc., New York, 1957) Chapter 10.
11. A more detailed report of this work has been submitted to Particle Accelerators.

TABLE I

Summary of the dimensions for the two helical resonators described in the text. Refer to Fig. 1 for definitions of a, c, L and s. Also given are the frequency of the lowest mode, $F_{exp.}$, and the corresponding frequency, F_s, predicted by the standard sheath model (ref. 6). $F_{calc.}$ and the α's are the result of the theoretical calculations.

a)

	Resonator A	Resonator B
a (cm)	2.15	5.40
c (cm)	7.47	16.19
L (cm)	19.82	14.60
s (cm)	0.903	2.043

b)

Resonator	$F_{exp.}$ (MH_z)	F_s (MH_z)	Approx.	N	$F_{calc.}$ (MH_z)	α_3/α_1	α_5/α_1	α_7/α_1	α_9/α_1
A	86.12	79	"half"	5	87.68	.255	-.065	.050	-.001
			"	10	87.20	.241	-.055	.045	-.008
			"full"	5	88.52	-.217	-.088	-.038	-.011
			"	10	88.16	-.206	-.081	-.034	-.014
B	49.26	38	"half"	5	46.14	.116	.001	.001	.000
				10	46.00	.115	.001	.001	.000
			"full"	5	51.78	-.076	-.004	-.000	.000
				10	51.66	-.074	-.004	-.000	.000

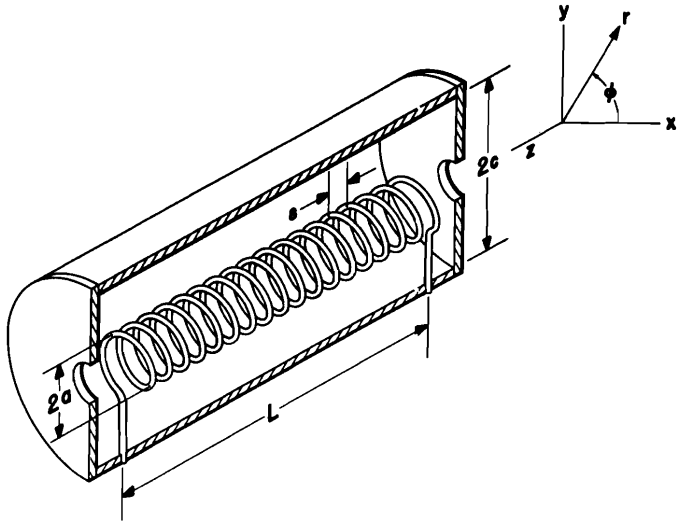

Fig. 1: A schematic drawing of a helical resonator that defines the dimensions and the coordinate system that are used in Section III. The space shown between the ends of the helix and the end walls of the cavity has been exaggerated for clarity; in resonators A and B this space has been kept to a minimum.

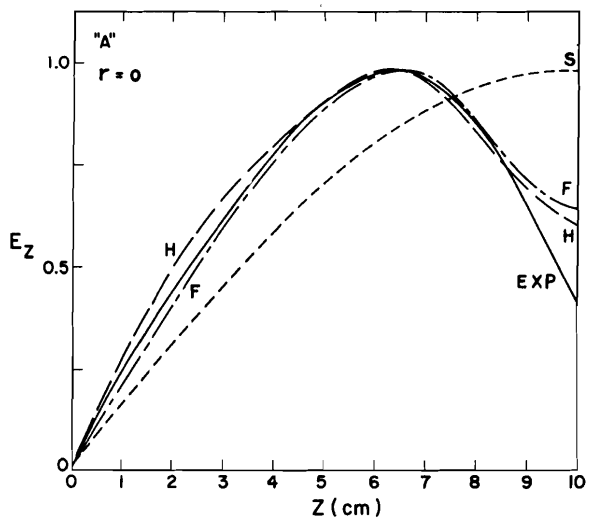

Fig. 2: The z component of the electric field, $E_z(0,z)$ in cavity A (see Table I for dimensions) along the axis of the cavity. The point z=0 corresponds to the center of the cavity; the helix is grounded at z=9.91 cm. The end wall of the cavity is at z=10.8 cm. The solid curve is the experimental result obtained using a dielectric bead; the dashed curve labeled S is the prediction of the standard sheath model. The curves labeled F and H are the results of using the "full" and "half" approximations, respectively. The magnitude of the field is given in arbitrary units and the four curves are normalized so as to give the same value at their maxima. (The F and H curves shown were calculated with N=5.)

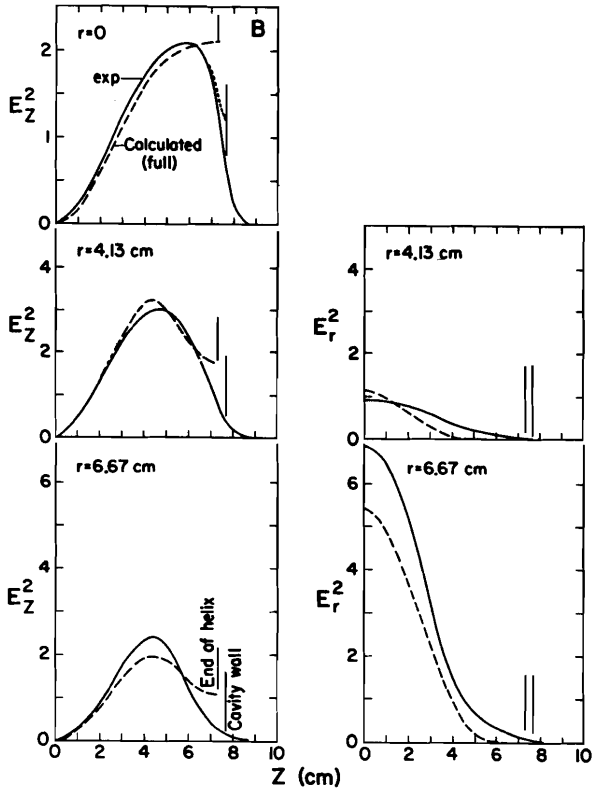

Fig. 3: The experimental values of E_r^2 and E_z^2 for cavity B obtained using the thin disk perturbation method are the solid curves. The dashed curves are the result of the "full" approximation with N=5. The normalization of the experimental and theoretical curves was obtained by matching the maxima in E_z^2 (r=0). The vertical lines indicate the positions of the end of the helix and the end wall of the cavity. The vertical scales give the correct relative magnitudes of the fields in arbitrary units. (The dotted addition to the experimental curve for E_z^2 (r=0) represents a crude attempt to correct for the finite size of the disk.)

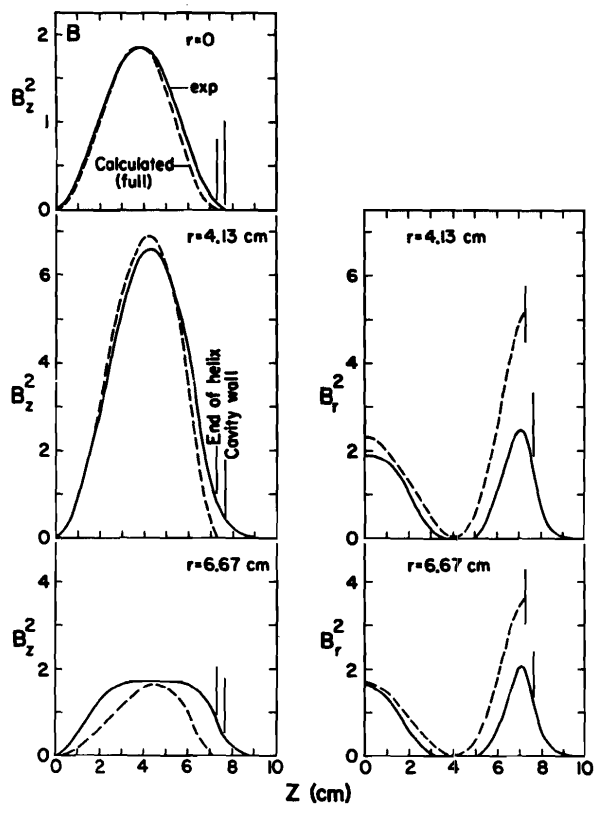

Fig. 4: The experimental values of B_r^2 and B_z^2 for cavity B obtained using the thin disk perturbation method are the solid curves. The calculations shown by the dashed curves use the "full" approximation with N=5. The relative normalization of the theoretical and experimental curves was made by matching the maxima of B_z^2 (r=0). The vertical lines indicate the positions of the end of the helix and the end wall of the cavity. The vertical scales give the correct relative magnitudes of the magnetic fields in arbitrary units.

DISCUSSION

Teng, NAL: What is the advantage of the helix over what you call the sheath model? Why don't people just build sheath-shaped drift tubes instead of the helix?

Bendt: The sheath shape model that the theory is based on is an infinitely thin conducting layer that has no space between turns. It simply has an anisotropic direction of conductivity and is an idealization of anything that you want to build which would have a finite thickness for structural purposes and for cooling water inside the helical tubes.

Teng: What is the physical advantage of the helix structure over the Alvarez structure? Isn't the alvarez structure similar to your sheath?

Bendt: I don't think so at all. What we have done is to shrink the dimensions of a resonant cavity by an order of magnitude over what the dimensions would be if it was not loaded by the helix. The velocity of an electromagnetic wave in this cavity is slower than the velocity in free space to a first approximation by the length of the helix to the length of the tubing which forms the helix. This can bring us down a factor of 50 if we have a large diameter and small spacing between the turns. So I think it in no way resembles an Alvarez drift tube type of structure.

Jones, ORNL: How closely does the actual axial electric field approximate a sign function and have you considered the effect of the real axial electric field on particle dynamics?

Allen, SLAC: In the abstract you mention considering the counterwound helix. Does that present some advantages or extend the range of beta over which you might operate?

Bendt: Yes. This was really a double helix, having two coupled modes. One of them has a very low β and it is easy to achieve a β of .02, but it turns out that the E fields on axis almost exactly cancel with high fields everywhere else, so when we got this device built we had a nice low β and no accelerating field.

Jones, ORNL: For the kind of machine that's being considered here, shunt impedance is only one consideration and the problem of flexibility is particularly important in matching different velocity profiles.

Lee, SLAC: Did you consider the effects of varying the pitch along the helix?

Bendt: We haven't done this experimentally, but we have considered varying the pitch with the possibility of achieving a larger shunt impedance. Since B_r is the cause of most of the losses, because the field is strongest between the turns, if we open up the helix in the middle and open it up at the end and compress it where B_r is zero, or very small, we feel that we could improve the shunt impedance.

Bendt: We don't see a sign function per se. We see something that peaks higher, having a substantial intersect, and a displaced maximum point. In response to your second question, the important feature is the beta of this structure or the equivalent half wavelength. We are incluned to think that you have to take the whole area under the curve and find its centroid in order to get some estimate, but we hope to determine this experimentally. At present, we haven't introduced this shape into any beam dynamics calculations.

Vogel, LASL: You said you have no free parameters in your theory to fit your measurements. Do your measurements satisfy Maxwell's equation?

Bendt: The theory satisfies Maxwell's equations for the idealized model that the theory is applied to. The perturbation measurements, which assume that the perturbation is small except where whatever we are drawing through the cavity parallel to the axis is either very close to the helix or very close to the end plates, presumably indicate to us the field

that would be there if the perturbing element was not there. But in that case Maxwell's equations are not exactly satisfied because there are additional boundary conditions due to the perturbing material. But the sphere is quite small (the sapphire sphere is 3/8 in. and the aluminum disks are .33 in.) compared to the size of the cavities, which are about 10 and 12 in. in diameter.

Vogel: Did you ever make an assessment as to which is actually the most reliable or the more accurate method; to develop the theory and believe it or do your perturbation measurements knowing that there is something not quite right?

Bendt: There are, of course, some errors in both. In the perturbation measurements we think we know what part of the curves are unreliable (it's the ends of the curves, for example). The theory is pretty good and is so much of an improvement over previous theories of this type that we feel it is useful enough to go ahead and use for design purposes.

Loew, SLAC: Do you know at this point over what range of velocities the helix is useful in terms of shunt impedance?

Bendt: We feel it is probably useful for β ranging from .02 to .08. For β greater than .03 we can get shunt impedances of 20 to 25 MΩ/meter; and for a β between .03 and .02 we may go down to 12 MΩ/meter in shunt impedance.